Engineering Failure Analysis 101 (2019) 309–319

Contents lists available at ScienceDirect

Engineering Failure Analysis

journal homepage: www.elsevier.com/locate/engfailanal

Investigation and analysis of finger breakages in commercial crystalline silicon photovoltaic modules under standard thermal cycling test

Subinoy Roy*, Sagarika Kumar, Rajesh Gupta

Department of Energy Science and Engineering, Indian Institute of Technology Bombay, Mumbai, India

ARTICLE INFO

Keywords:
PV module
Finger breakage
Thermal cycling test
Electroluminescence imaging
Distributed diode model
Failure analysis

ABSTRACT

The front grid fingers play a major role in the conduction of current in crystalline silicon photovoltaic (PV) modules. These fingers generally break with time during the field exposure which affects the modules mechanical and electrical integrity and causes reduction in its performance. In this paper, a systematic methodology has been presented for investigation of the nature and evolution of finger breakages observed in crystalline silicon PV technology modules under standard thermal cycling tests as specified under IEC 61215 standard. Illuminated current-voltage (I-V) analysis and electroluminescence (EL) imaging techniques have been exploited in tandem for investigation of the cause, types and progression of the finger breakages. The results obtained from the study identified various faulty solder configurations which are sensitive to thermal fatigue and subsequently cause finger breakages. A generalized method to quantify the finger breakages from EL images has been introduced. The different finger breakage patterns have been classified according to their appearance in the EL images originating from the breakage of the busbar-finger junctions. Distributed diode modelling and simulation have also been performed for the quantification of severity of different finger breakage patterns. In addition, a finger breakage constant has been proposed for comparative assessment of durability of fingers in PV modules under thermal cycling test conditions. The present investigation and analysis of finger breakages can be instrumental in prevention of failures thereby enhancing performance and durability of PV modules.

1. Introduction

A photovoltaic (PV) module structure consists of a packaged assembly of interconnected solar cells, where each part plays an important role in maintaining its overall performance. In commercial crystalline silicon PV modules, front grid fingers in the cells allow the collection of current generated in the cell to the busbars and also accommodate collection from regions far from the busbars. In this manner, fingers contribute in maintaining the electrical integrity within a module. Any structural damage to the fingers at manufacturing stage or under harsh environmental conditions in the field induce cracks in them which are generally termed as finger breakages. The breakage of such fingers affects the current conduction in the module which increases the series resistance and decreases the fill factor that ultimately reduces the module performance. Fresh PV modules generally do not suffer from finger breakages however during long term field exposure, modules face thermo-mechanical fatigue which leads to such breakages [1,2].

* Corresponding author.
E-mail address: subinoy@iitb.ac.in (S. Roy).

https://doi.org/10.1016/j.engfailanal.2019.03.031
Received 30 December 2017; Received in revised form 11 March 2019; Accepted 27 March 2019
Available online 28 March 2019
1350-6307/

The breakages affect the mechanical stability of fingers which hinders its current carrying capability and hence, reduces the overall performance and can induce premature failure in the modules.

In the present scenario when huge module installations based on crystalline silicon PV technology are underway, detection and analysis of sources of premature failures is an important aspect. To be able to address an important part of this concern, there is a need for in-depth analysis of finger breakages in commercial crystalline silicon PV modules. For the purpose of facilitating thermal fatigue within PV modules, IEC 61215 standard provides for thermal cycling (TC) test which checks for the modules capability to withstand thermo-mechanical mismatch produced due to the alternating temperature ramping cycles [3–5]. The solder material has been reported to be particularly vulnerable to temperature cyclic variations [6–8], as it generates creep strain under such conditions. The accumulated strain causes the creation of cracks at the solder material which subsequently induces breakage in the metal fingers near the busbar-finger junctions [9,10].

In this work, a detailed analysis of the finger breakage in commercial crystalline silicon PV modules has been performed by using standard thermal cycling test conditions. Electroluminescence (EL) imaging [11,12] and illuminated current-voltage (I-V) analysis [13,14] have been used in tandem for the in-depth analysis of finger breakages. The combination of these characterization techniques provide the advantage to correlate the nature of breakages in correspondence to each other. The information obtained from these techniques have been analysed to understand the impact, evolution and progression of finger breakages with the thermal cycles, which can be instrumental in mitigation of such defects early at production level. The study has been channelized to understand the cause of finger breakages and its different classifications in detail. A novel finger breakage constant has been devised for a comparative assessment of durability of fingers in PV modules.

2. Methodology

A systematic approach has been developed to carry out the finger breakage analysis in crystalline silicon PV modules. Commercial PV modules from different manufacturers have been subjected to standard TC, as per IEC 61215 standard. These modules have initially been characterized by I-V technique to obtain the output power and other electrical parameters for reference. EL imaging has also been performed for spatial mapping of the defects present in the modules. TC has been performed in multiple stages to observe the appearance and progression of finger breakages in the PV modules. I-V analysis and EL imaging have been carried out at each intermediate stages to characterize the defects generated after the tests. In order to support the experimental findings, additional tests have been performed on encapsulated solar cell samples to investigate the finger breakage patterns in the EL images. The observed finger breakage types have been categorized according to their appearance in EL images and a generalized approach for their quantification from the EL images has been proposed. In order to estimate the relative impact of these finger breakages, distributed diode model of solar cell has been simulated using PSpice circuit simulator. To understand the progression of finger breakages with thermal cycles, additional cycles have been performed on modules to establish a generalized relation between the finger breakages with number of cycles.

3. Experimental

In order to investigate the finger breakages in PV modules, standard TC has been performed on a total of 8 modules from 4 commercial crystalline silicon PV manufacturers (two modules each). The modules have been named as M_{mn}, where m stands for the manufacturer number (1 to 4) and n stands for sample number 1 and 2 of each manufacturer. The modules have been chosen to have comparable electrical and geometrical parameters. All the modules consist of 36 series connected cells, which have output power in the range of 30 W to 40 W and area in the range of 0.25 to 0.35 m^2.

The modules have been subjected to 200 thermal cycles according to the IEC 61215 standard. To investigate the fine progression of finger breakages with time, the test has been performed in four consecutive stages of 50 cycles each. Each cycle is of 5 h having

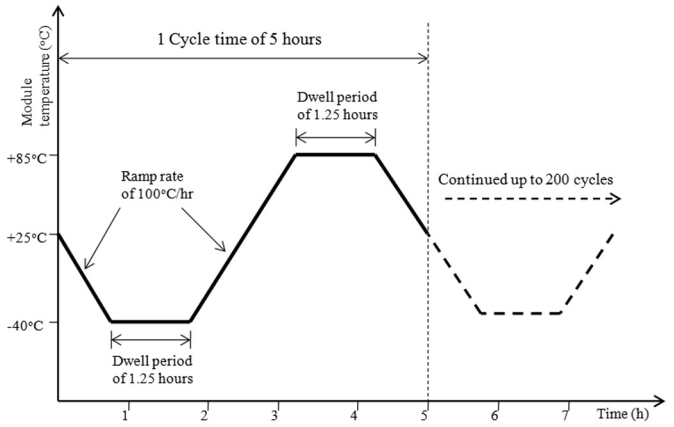

Fig. 1. Time profile of thermal cycles.

maximum and minimum temperatures of +85 °C and −40 °C respectively, with a ramp rate of 100 °C/h and dwell period (constant temperature) of 1.25 h each at +85 °C and −40 °C. The time profile of each thermal cycle is shown in Fig. 1. A standard environmental chamber (Weiss, WKS 3–1500/70/5) designed for PV module testing has been used to perform the test.

In order to investigate the change in maximum output power (P_{max}) of the modules under the test along with change in other electrical parameters viz. short circuit current (I_{sc}), open circuit voltage (V_{oc}), series resistance (R_s) and the fill factor (*FF*), I-V analysis has been performed using a solar simulator. The measurements have been performed under standard test conditions (STC) of AM 1.5G, 1000 W/m^2 and 25 °C. The R_s has been measured from I-V curve of the PV modules. Built-in software of solar simulator calculates the R_s from the slope of I-V curve near V_{oc}. The repeatability of the simulator was good, which was less than 1% for all the measurements. The measurements have been performed under similar spatial and ambient conditions to minimize the error due to geometrical and environmental factors.

For investigation and spatial analysis of finger breakages in PV modules, EL imaging has been performed. In the experimental setup, an EL camera has been used that has a silicon based charged couple device (Si-CCD) detector of 1024 × 1024 pixels resolution, which is sufficient for spatial analysis of the finger breakages in this study. The camera has been actively cooled by forced air circulation to increase signal to noise ratio in the measurement. The camera has been connected to an externally programmed power supply (TDK-Lambda, GEN150–10) that is used to bias the modules. A monitoring PC has been used to control the EL operation. The entire system has been synchronized optimally to obtain a good quality image. The overall setup has been placed inside a dark chamber in order to minimize stray light and the chamber has been kept at a constant temperature of 25 °C to maintain similar conditions for all the measurements. For a comparative analysis of EL images, the modules have been operated under constant current mode at rated I_{sc} value of the respective modules.

The finger breakages identified in the EL images have also been investigated by a digital microscope (resolution of 1600 × 1200 pixels) that enables detailed visual inspection at a magnified view to the order of up to 500× of the cell sample.

4. Results and discussion

In this section, the investigation on evolution and progression of finger breakages under the TC test has been presented and analysed in detail by experimental results obtained using visual inspection, I-V measurement and EL imaging technique.

4.1. Initial defect investigation on PV modules

Initial investigation for detection of pre-existing defects in the PV modules before the TC test has been performed using EL imaging. This initial investigation identified two types of dominant defects. First type of defect was on the finger grid and second type were micro-cracks on the silicon wafer. The defects observed on the finger grids were further classified into two types depending on the location and pattern visible in the EL images. The first type were finger cuts, which appeared as dark rectangular shaped regions that originated from cut locations along the affected finger in the EL images, as shown in Fig. 2(a). These finger cut locations were visually observed as discontinuation in the finger lines and were commonly found within the investigated modules. The second type of finger defects were identified as finger breakages in the modules, those were visible as dark rectangular shaped regions that originated near the busbar-finger junctions (common connecting point of busbar and finger) under the copper ribbon, as shown in the

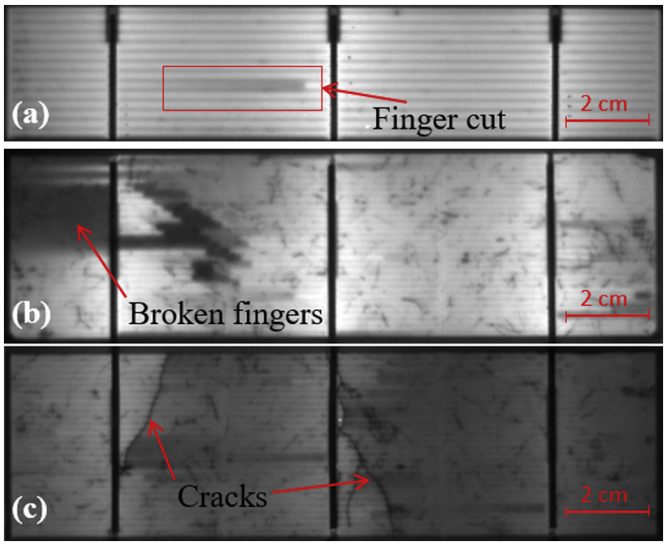

Fig. 2. Types of defects observed in EL imaging of PV modules before thermal cycling test: (a) finger cut; (b) finger breakages and (c) cracks on the wafer originating from the busbar.

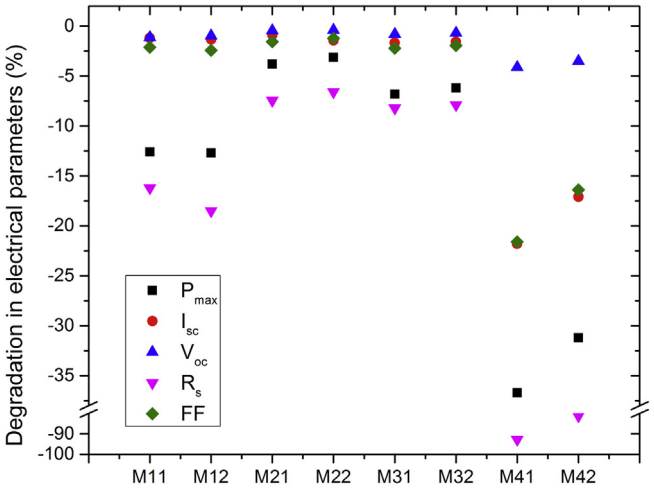

Fig. 3. Degradation in electrical parameters of modules after 200 thermal cycles.

EL image in Fig. 2(b). The finger breakages were difficult to locate visually without a microscope unlike the finger cuts. However, they were easily differentiable in EL images according to the location of origin of the dark rectangular pattern. Both the types of finger defects (Fig. 2) were observed to appear in a random spatial distribution across the cells of the investigated modules.

In addition to the finger defects, some of the investigated modules also showed cracks on the silicon wafers, visible as dark irregular line shaped pattern in the EL images, as shown in Fig. 2(c). These cracks may have appeared due to mechanical imbalance in the module structure or stress generated at the solder junctions during the fabrication process [15–20]. The majority of cracks observed in the investigated modules originated from the busbar, which indicates that these cracks are most likely solder induced.

4.2. Investigation after thermal cycling test

The deterioration in module electrical parameters after 200 thermal cycles is presented in Fig. 3. Varying power drops in the modules is observed; where the least drop (less than 4%) is observed in M2 module samples and highest drop (more than 30%) in M4 samples. The sample modules from each batch have shown similar power drop. The power drop in the modules can be attributed to deterioration of other electrical parameters. R_s is identified as the most affected parameter whereas V_{oc} is the least affected, as observed in Fig. 3. The significant change in R_s indicates that the current carrying paths in the modules have been significantly affected while negligible reduction in V_{oc} indicates that the shunt resistances in the modules have not been affected much. Therefore, from the I-V analysis, increase in R_s is identified as the global degradation mode under TC test conditions.

The EL images of one sample module from each module batch before and after 200 cycles is shown in Fig. 4. The images dominantly indicate appearance of dark rectangular shaped regions that originated from the busbar-finger junctions, identified as front grid finger breakages. The finger breakages appeared in a variable extent in the different module samples, where the maximum number of breakages appeared in M4 modules. In addition to the new breakages, the pre-existing finger breakages in the modules also deteriorated under the test conditions, visible as increased area and reduced EL intensity of the existing dark rectangular patterns. The appearance and deterioration of finger breakages in the modules supported the large extent of increment in R_s and also decrement in *FF* and module power in the I-V analysis results.

Apart from finger breakages, the pre-existing cracks are observed to deteriorate under the test, as seen in M2 and M3 modules (Fig. 4). This deterioration is distinguishable by drop in EL intensity across the cracked area and also the completely separated cell areas. The deterioration is observed to be location specific, where only the pre-existing cracks located near the busbar-finger junctions are affected, but no new cracks appeared. The appearance of finger breakages and deterioration of cracks identified the busbar-finger junctions to be the most vulnerable to the thermal fatigue under the test. Apart from these two defect types, there are other possibilities of degradation under the test such as generation of micro-cracks at different module layers, degradation of material quality or any structural damage which may not be visible in the EL images but can also contribute to power loss. However, the present study has been focussed on the analysis of finger breakages only.

4.2.1. Effect of solder configuration on finger breakages

The breakage in fingers under thermal fatigue occurs due to the difference in temperature coefficient between the silicon cell and the solder coated copper ribbon [10]. In this context, the solder configuration in the module samples and its corresponding effect on the finger breakages has been investigated. A commercial multi-crystalline cell has been encapsulated by soldering the ribbons partially on top of the busbars. This configuration essentially creates a soldered and a solder free region in the cell. This encapsulated cell has been exposed to 100 TC test. The EL images (Fig. 5) after the test show that the breakages appeared only at the soldered region while the solder free regions did not generate any breakage. It indicates that the solder configuration is a crucial parameter for

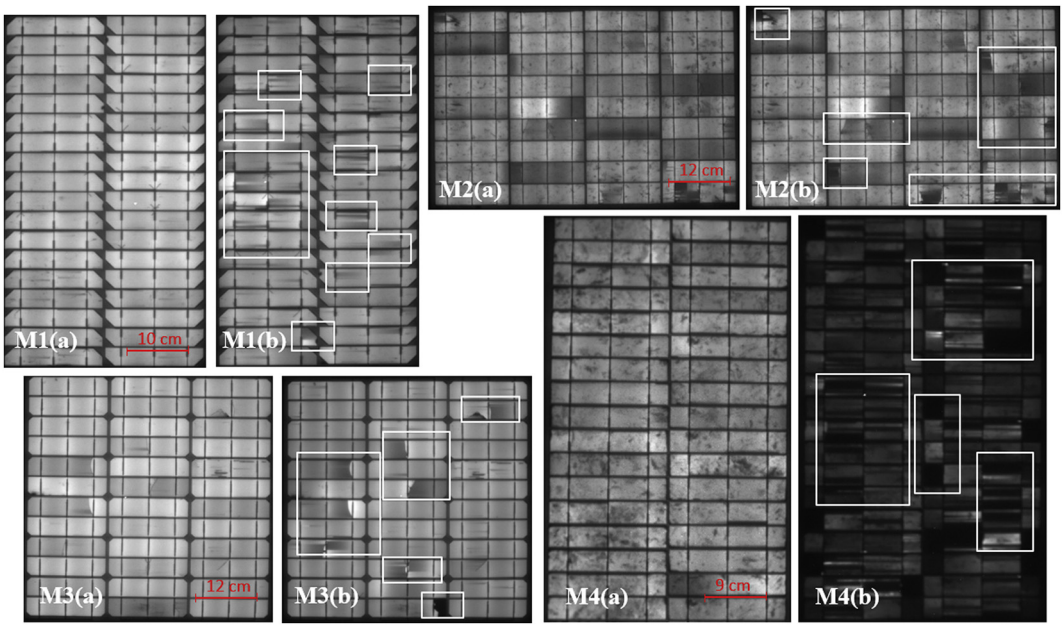

Fig. 4. EL images of different sample modules (a) before and (b) after 200 thermal cycles.

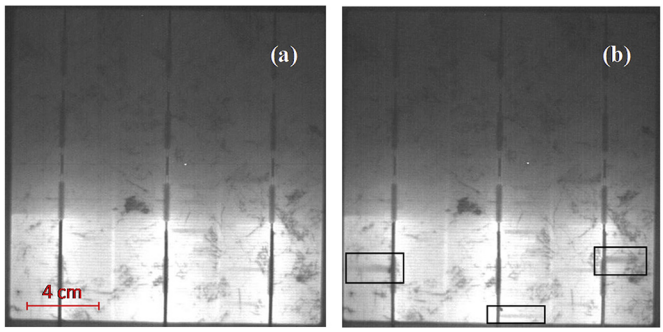

Fig. 5. EL images of encapsulated cell with partially soldered ribbon (a) before and (b) after 100 thermal cycles, indicating the appearance of finger breakages.

creation of finger breakages under TC test.

The solder configurations in the module samples have also been visually investigated. Different quality of soldering in the cells of a module sample are shown in Fig. 6, such as a good soldered ribbon (Fig. 6a), a faulty soldered ribbon where excess solder material spread out at the vicinity of the ribbon on top of the fingers (Fig. 6b), dripping of excess solder material on top of the fingers (Fig. 6c) and a dislocated ribbon (Fig. 6d). All the investigated modules showed these types of faulty solder configurations in varying extents. It has been observed that at these locations more finger breakages have been generated after the TC test in all the module samples, which indicates these types of poor solder configurations generate finger breakages near the busbar-finger junctions. This can also be used to explain the pre-existing finger breakages observed in the module samples (Fig. 2) initially before TC test, which may have possibly appeared during the ribbon tabbing process where the excess solder material could have caused breakage during its cooling down to ambient temperature.

It has also been observed that the dislocated ribbon caused the maximum amount of finger breakages among other faulty solder configurations. To further investigate the extent of severity of finger breakages due to ribbon dislocation under the TC test, an experiment has been designed. A multi-crystalline encapsulated cell with slightly deviated ribbons (on top of the busbars) was subjected to 100 TC test. The EL image after the test (Fig. 7) shows that significant amount of finger breakages appeared only at the side of the busbars where the ribbon touches the respective busbar-finger junctions. The significant influence of dislocated ribbons on finger breakages explains the appearance of wide dark rectangular patterns in EL images of the sample modules (Fig. 4, M4b). It can be inferred that the ribbon tabbing is a crucial process in PV manufacturing and special care should be taken while soldering the ribbons on top of busbars in order to minimize finger breakages.

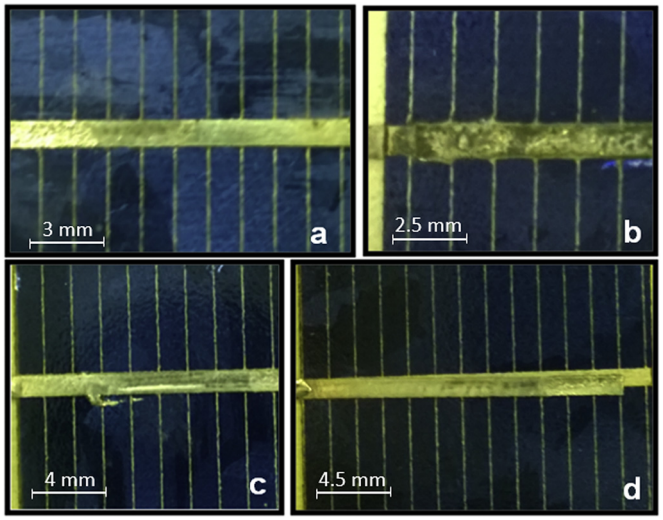

Fig. 6. Types of soldering configurations visually observed in the cells: (a) good soldered ribbon; (b) excess solder material in the vicinity of the ribbon; (c) excess solder material dripped over the finger and (d) dislocated ribbon on top of busbar.

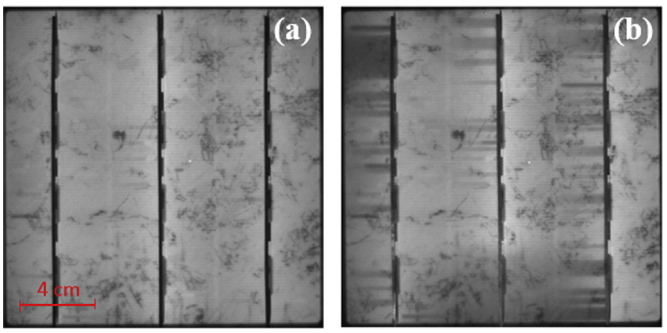

Fig. 7. EL images of encapsulated cell with dislocated interconnecting ribbons (a) before and (b) after 100 thermal cycles.

4.3. Analysis of finger breakages

In this section, classification and quantification of finger breakage patterns observed in the EL images and the corresponding impact of the classified breakage patterns on the cell performance has been investigated. For the purpose of representation, a methodology for quantification of the fingers has been developed, which has been used in the further sections. Since the finger breakage occurs due to formation of cracks near the busbar-finger junctions, the number of such junctions is the potential countable parameter. The count in a cell can be represented as $2N_{BB}N_{Fin}$ where N_{BB} and N_{Fin} are the number of busbars and fingers in the cell respectively. Likewise in the module, the count is $2N_{BB}N_{Fin}N_{Cell}$ where N_{Cell} is the number of cells in the module. Sample M4 modules have been chosen for the abovementioned analysis as it displayed all varieties of finger breakage patterns.

4.3.1. Classification and quantification of finger breakage patterns

The finger breakage patterns have been classified into three distinct types, on the basis of affected junction location and the patterns visible in EL images, as depicted in the zoomed EL image of a part of a module (Fig. 8). The first types (Type A) are the partially affected fingers that are observed in between two busbars. In this case, the breakage occurs in the busbar-finger junction at either end of the finger. A major amount of current flows through the finger from the other intact end, thus appears partially dark with diminished EL intensity along the finger length. These are the most common breakage types found in the intermediate stages of TC test. The second types (Type B) are the fully affected fingers, also observed in between two busbars. Here, the busbar-finger junctions at both end of the finger get broken. Hence, lack of current from both directions produces reduced EL intensity across the entire finger length. The third types (Type C) are the broken busbar-finger junctions at outer side of the busbars where the fingers are connected to the cell edges. In this case, the only available conduction path from the busbars get affected, thus appear dark across entire finger length in the EL images.

Varying crack widths at the busbar-finger junctions had been observed under TC test condition, as shown in the microscopic image of a sample soldered cell exploited under TC test (Fig. 9). It has also observed from the EL images in Fig. 8 that the drop in EL intensity across the affected fingers for individual breakage types varies. As an example, a significant difference in drop in EL

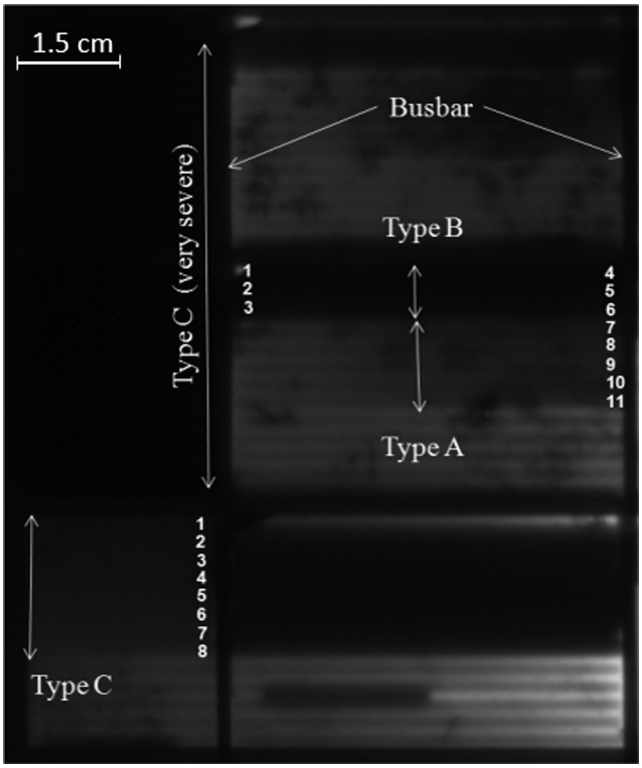

Fig. 8. Zoomed EL image of cells showing type A, B and C finger breakages and their counting methodology.

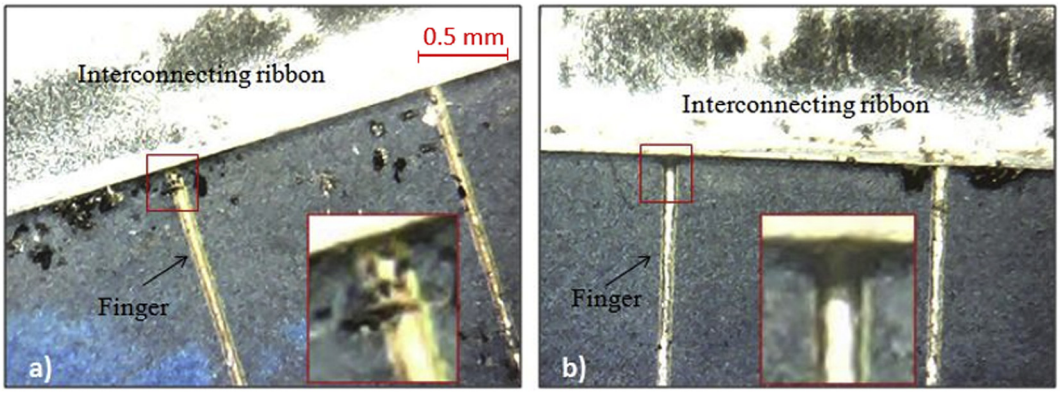

Fig. 9. Microscopic images of a (a) partially detached and a (b) fully detached finger in a cell.

intensities of type C breakages at two different locations can be seen in Fig. 8. The varying EL intensities may be due to the variable width of the cracks generated at the busbar-finger junctions after the test that provides different resistive path for the current flow to the fingers during EL operation.

The quantification of the finger breakage types has been shown in Fig. 8, where the individual broken fingers have been assigned numbers. The count of the broken fingers for different breakage types have been identified from the width of the dark rectangular pattern. In such a manner, type B is considered as two breakages and type A and type C as one breakage each. This counting procedure has been used in the following sections to calculate the number of finger breakage patterns in the modules.

4.3.2. Impact analysis of finger breakage patterns

In order to study the impact of different finger breakage patterns (Type A, B and C), a distributed diode model of solar cell has been simulated using PSpice circuit simulator. Such simulation approach has been used in literature to study the effect of different electrical parameters on solar cell performance [21–24]. In this approach, the solar cell has been divided into large number of elementary areas (150 × 30) and each elementary area has been modeled using its electrical equivalent circuit, comprising of a diode, a current source and a parallel resistance. The number of elementary areas has been chosen considering the finger and busbar

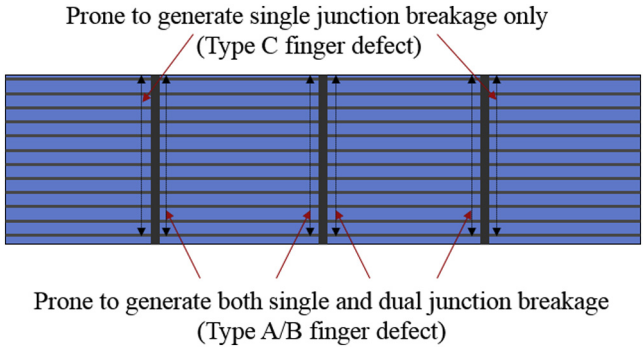

Fig. 10. Location of different types of finger breakages (Type A, B and C) introduced in simulation in a three-busbar single solar cell.

width and the optimum computational time. Electrical parameters of each elementary area has been obtained from an actual crystalline silicon solar cell. The fingers and busbars have been modeled according to their respective measured resistances and the lateral resistance of the emitter has been estimated from the measured sheet resistance. The other parameters; the reverse saturation current (I_0) and diode ideality factor (n) have been obtained from the dark I-V characteristics of the actual cell.

Finger breakages at the intersection of the busbars and fingers has been introduced in the model by a high resistance at the corresponding locations. The respective location of introduction of the three breakage types is depicted in Fig. 10. A constant resistance value has been considered in the simulation to relate the trend of loss in output power with finger breakages. The loss in output power with increasing number of finger breakages, for the three breakage types is shown in Fig. 11. Simulation has been performed in steps of 5% for breakages up to 30%, which is a significantly large number in practical aspect. The figure shows that the percentage loss in output power increases in a non-linear manner with increasing number of breakages for these individual breakage types. The Type A shows least loss whereas Type C shows the highest. It can be explained as in case of Type A, the breakage occurs near a busbar-finger junction in between two bus-bars. For this type, the current still flows through the other intact end unlike Type B breakage, and results in lesser power drop. If both the ends break (Type B), the entire finger becomes nearly inactive and more power loss occurs in comparison to Type A. In case of Type C, a single breakage at the busbar-finger junction leads the entire finger nearly inactive that results in more severe power loss in comparison to other two breakage types.

4.3.3. Progression of finger breakages with thermal cycles

In this section, the progressive trend of finger breakages with thermal cycles has been investigated. The module batch with sufficiently high number of breakages has been chosen (M4 sample modules) for investigation. The EL images of one sample module at all intermediate stages of TC has been presented in Fig. 12. The figure shows that all the finger breakage patterns appeared in the module in a random spatial distribution. For a simplified representation, the distribution of finger breakages in individual cells of the module with progressive test stages have been quantified (following Section 4.3.1) and represented in Fig. 13. The numbers in the figure represent the percentage breakage of the total number of fingers in a cell. The greyscales differentiate varying percentage where, the darker scales represent higher numbers. The difference in amount of finger breakages in the individual cells (Fig. 13) may be attributed to the difference in quality of soldering. The representation also shows a drastic increment in number of breakages in

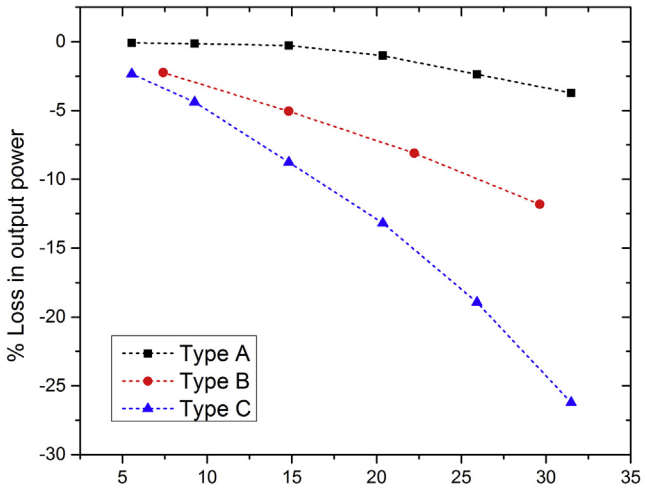

Fig. 11. Trend of loss in output power in a cell with finger breakages, for type A, B and C breakages.

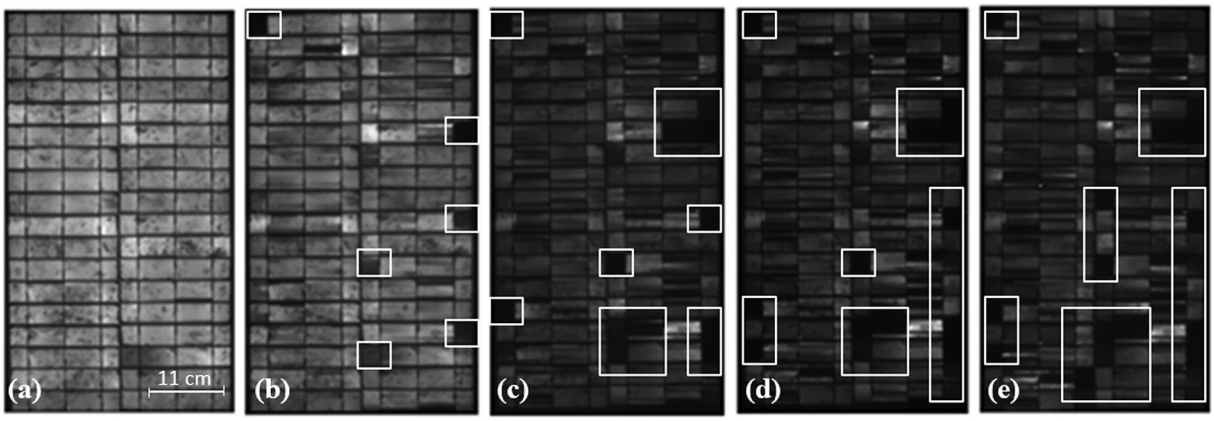

Fig. 12. EL images of sample module under thermal cycling test; (a) before and after (b) 50 (c) 100 (d) 150 and (e) 200 thermal cycles, indicating deterioration of finger breakage patterns.

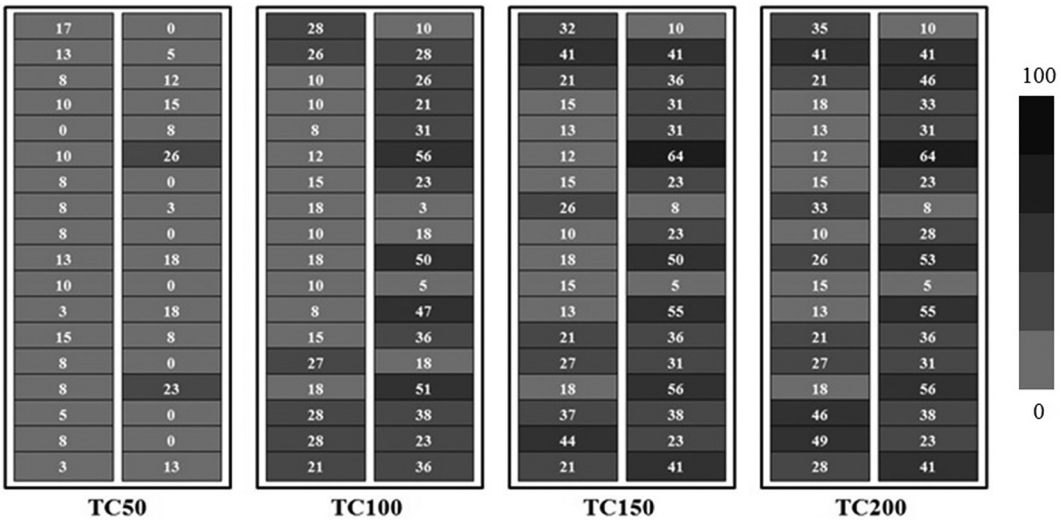

Fig. 13. Distribution and progression of finger breakages quantified (in percentage) at different test stages across the cells in the module.

different cells up to 100 cycles and a comparatively fewer increment at later stages (from TC150 to TC200). This indicates a global saturating tendency of finger breakages at module level with progressive thermal cycles.

To further investigate the saturating tendency of finger breakages, additional 200 thermal cycles have been performed on these modules at regular intervals of 50 cycles. The number of intact or non-broken fingers (N_F) at intermediate stages of the test have been calculated by identifying the number of broken fingers (N_{FB}) and following the equation,

$$N_F = N_{F0} - N_{FB} \tag{1}$$

Where N_{F0} is the initial number of non-broken fingers before the test. Fig. 14 represents the decreasing trend in total number of non-broken fingers for two sample modules up to 400 cycles. The trend shows a drastic decrement in the number of non-broken fingers at initial cycles and saturating nature at higher cycles. The observed nature of relationship between the numbers of non-broken fingers (N_F) with thermal cycles (N_C) can be represented as,

$$N_F = \alpha\, e^{-\beta N_C} \tag{2}$$

Where α is the initial number of non-broken fingers in the module, i.e. N_{F0} and β is a constant related to the soldering characteristics and the test parameters which is directly related to the durability of the fingers in the module. The Eq. (2) can be represented as,

$$N_F = N_{F0}\, e^{-\beta N_C} \tag{3}$$

Differentiating Eq. (3),

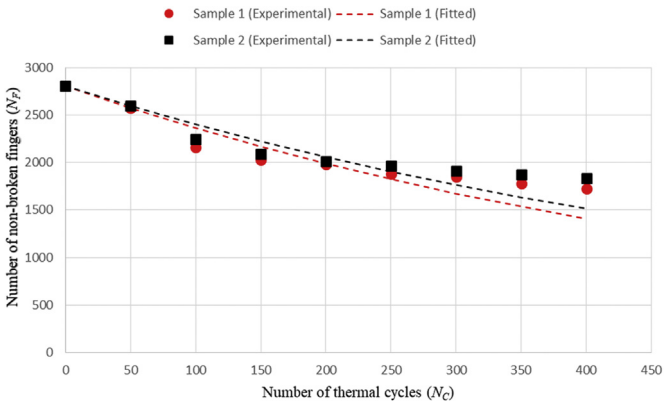

Fig. 14. Trend between numbers of non-broken fingers with thermal cycles.

$$\frac{\Delta N_F}{\Delta N_C} = -\beta N_F \tag{4}$$

The Eq. 4 represents the degradation rate of finger breakages under TC test. It is linearly dependent on the number of non-broken fingers (N_F) at any instance (N_C) of the test. The constant term β is defined as the finger breakage constant which is a key performance deterministic parameter in the modules. It can be used for comparative assessment of durability of fingers between different modules, under TC test conditions. Combining Eq. (1) and (3), β is estimated as,

$$\beta = \frac{1}{N_C} ln \frac{N_{F0}}{N_{F0} - N_{FB}} \tag{5}$$

The β indicates the global soldering quality in a PV module. The lower is the β, the higher is the durability of fingers in a particular PV module. The trend of non-broken fingers with thermal cycles has been fitted considering the initial number of non-broken fingers and the average value of the experimentally obtained β, as shown in Fig. 14.

5. Conclusions

In this paper, a detailed analysis on finger breakages in crystalline silicon PV modules under standard thermal cycling test has been presented. Electroluminescence (EL) imaging analysis has been exploited in tandem with illuminated current-voltage (I-V) analysis to investigate the cause, types, severity and progression of finger breakages. Increment in series resistance was identified as the global degradation mode under the thermal cycling test. Finger breakages were found to be the dominant defect type which spatially appeared in varying extents in the EL images of the investigated modules. Multiple faulty solder configurations with varying impacts on amount of breakages were recognized as the dominant causes of finger breakages; such as spilling of excess solder material and displaced interconnecting ribbon. The configuration with the dislocated ribbon on top of busbars produced the most significant amount of breakages, which was further supported with experiments conducted on an encapsulated cell sample. Distinct types of broken fingers were classified according to their appearance in EL images originating from the breakage of the busbar-finger junctions. The impact of these breakage types on cell performance showed that the broken busbar-finger junction connecting the busbar to the cell edge most significantly affects the cell performance. The finger breakages were observed to get saturated in modules with progressive thermal cycles. Extended cycle behaviour indicated a trend of an exponential decay of intact fingers due to breakage that achieved a global saturation at higher cycles. A finger breakage constant was deduced from this trend that can be instrumental for comparative assessment of durability of fingers and hence the quality of soldering in PV modules. The findings from this study can be helpful in setting guidelines for prevention of finger breakage failures in PV modules during both fabrication process and outdoor-installation.

References

[1] M.A. Quintana, D.L. King, T.J. McMahon, C.R. Osterwald, Commonly observed degradation in field-aged photovoltaic modules, Proceedings of the Photovoltaic Specialists Conference, Conference Record of the Twenty-Ninth IEEE, New Orleans, Louisiana, USA, 2002, pp. 1436–1439.
[2] M. Chicca, G. TamizhMani, Nondestructive techniques to determine degradation modes: Experimentation with 18 years old photovoltaic modules, Proceedings of the 42nd IEEE Photovoltaic Specialist Conference, New Orleans, LA, USA, 2015, pp. 1–5.
[3] Standard IEC 61215, Crystalline Silicon Terrestrial Photovoltaic (PV) Modules – Design Qualification and Type Approval, Geneva, Switzerland, (2005).
[4] C. Ferrara, D. Philipp, Why do PV modules fail? Energy Procedia 15 (2012) 379–387.
[5] R. Khatri, S. Agarwal, I. Saha, S.K. Singh, B. Kumar, Study on long term reliability of photo-voltaic modules and analysis of power degradation using accelerated aging tests and electroluminescence technique, Energy Procedia 8 (2011) 396–401.
[6] N. Bosco, T.J. Silverman, S. Kurtz, Climate specific thermomechanical fatigue of flat plate photovoltaic module solder joints, Microelectron. Reliab. 62 (2016) 124–129.
[7] N. Bosco, T.J. Silverman, S. Kurtz, The influence of PV module materials and design on solder joint thermal fatigue durability, IEEE J. Photovolt. 6 (6) (2016) 1407–1412.

[8] S. Kumar, R. Gupta, Investigation and analysis of thermo-mechanical degradation of fingers in a photovoltaic module under thermal cyclic stress conditions, Sol. Energy 174 (2018) 1044–1052.
[9] N. Park, J. Jeong, C. Han, Estimation of the degradation rate of multi-crystalline silicon photovoltaic module under thermal cycling stress, Microelectron. Reliab. 54 (8) (2014) 1562–1566.
[10] P. Chaturvedi, B. Hoex, T.M. Walsh, Broken metal fingers in silicon wafer solar cells and PV modules, Sol. Energy Mater. Sol. Cells 108 (2013) 78–81.
[11] T. Fuyuki, A. Kitiyanan, Photographic diagnosis of crystalline silicon solar cells utilizing electroluminescence, Appl. Phys. A Mater. Sci. Process. 96 (1) (2009) 189–196.
[12] A. Sinha, O.S. Sastry, R. Gupta, Nondestructive characterization of encapsulant discoloration effects in crystalline-silicon PV modules, Sol. Energy Mater. Sol. Cells 155 (2016) 234–242.
[13] K.M. Lin, Y.H. Lee, W.Y. Huang, Y.W. Kuo, L.K. Wang, S.Y. Yang, Long term reliability and power degradation analysis of multicrystalline silicon solar modules using electroluminescence technique, Adv. Mater. Res. 562 (2012) 90–93.
[14] J.M. Delgado-Sanchez, E. Sanchez-Cortezon, C. Lopez-Lopez, R. Aninat, M.D. Alba, Failure mode and effect analysis of a large scale thin-film CIGS photovoltaic module, Eng. Fail. Anal. 76 (2017) 55–60.
[15] M.A. Munoz, M.C. Alonso-Garcia, N. Vela, F. Chenlo, Early degradation of silicon PV modules and guaranty conditions, Sol. Energy 85 (9) (2011) 2264–2274.
[16] M. Köntges, I. Kunze, S. Kajari-Schrder, X. Breitenmoser, B. Bjørneklett, The risk of power loss in crystalline silicon based photovoltaic modules due to micro-cracks, Sol. Energy Mater. Sol. Cells 95 (2011) 1131–1137.
[17] S. Kajari-Schröder, I. Kunze, U. Eitner, M. Köntges, Spatial and orientational distribution of cracks in crystalline photovoltaic modules generated by mechanical load tests, Sol. Energy Mater. Sol. Cells 95 (2011) 3054–3059.
[18] S. Pingel, Y. Zemen, O. Frank, T. Geipel, J. Berghold, Mechanical stability of solar cells within solar panels, Proceedings of the 24th European Photovoltaic Solar Energy Conference, WIP, Dresden, Germany, 2009, pp. 3459–3464.
[19] B. Kang, N. Park, S.J. Tark, W.W. Oh, S. Park, Y. Do Kim, H.S. Lee, D. Kim, Advanced yield strength of interconnector ribbon for photovoltaic module using crystallographic texture control, Met. Mater. Int. 20 (2014) 229–232.
[20] A. Kilikevičius, A. Čereška, K. Kilikevičienė, Analysis of external dynamic loads influence to photovoltaic module structural performance, Eng. Fail. Anal. 66 (2016) 445–454.
[21] P. Somasundaran, R. Gupta, Influence of local shunting on the electrical performance in industrial silicon solar cells, Sol. Energy 139 (2016) 581–590.
[22] S. Roy, P. Somasundaran, R. Gupta, Estimation of shunt resistance by electroluminescence imaging, Proceedings of the 29th European Photovoltaic Solar Energy Conference and Exhibition, Amsterdam, Netherlands, 2014, pp. 1224–1227.
[23] A. Zekry, A.Y. Al-Mazroo, A distributed SPICE-model of a solar cell, IEEE Trans. Electron Dev. 43 (5) (1996) 691–700.
[24] B. Galiana, C. Algora, I. Rey-Stolle, I.G. Vara, A 3-D model for concentrator solar cells based on distributed circuit units, IEEE Trans. Electron Dev. 52 (12) (2005) 2552–2558.